Frequenz
57 (2003)
11-12

Design and Realisation of a Compact 38 GHz Radiometer

Entwurf und Realisierung eines kompakten 38 GHz Radiometers

Abstract
Architecture, design, assembly and performance data of a 38 GHz radiometer are presented in this article. The radiometer is intended to serve as a demonstrator in microwave system education and as a platform to demonstrate novel RF structures and design techniques. Among other components, it includes a folded planar reflect array antenna, a mechanically sealed transition from circular waveguide-to-microstrip and several monolithic microwave integrated circuits (MMIC). With an internal reference and various analog and digital compensation circuits, the radiometer is able to measure absolute noise temperatures within a considerable operating temperature range. Adjustable data integration parameters allow the radiometer to be used for many different scenarios. The overall performance of the radiometer is verified by system measurements and some exemplary field tests.

Übersicht
In diesem Artikel werden Architektur, Entwicklung und Aufbau eines Radiometers bei einer Frequenz von 38 GHz beschrieben. Das Radiometer stellt sowohl ein Demonstrationsobjekt in der Lehre als auch eine Experimentierplattform für neue Hochfrequenzstrukturen und Entwurfstechniken dar.
Es enthält unter anderem eine gefaltete planare Reflektorantenne, einen mechanisch dichten Übergang von Rundhohlleiter auf Mikrostreifenleitung und verschiedene MMIC-basierte Millimeterwellen- und Hochfrequenzschaltungen. Da das Radiometer über eine interne Referenz und verschiedene analoge und digitale Kompensationsnetzwerke verfügt, ist die Messung von absoluten Rauschtemperaturen innerhalb eines beträchtlichen Gerätetemperaturbereichs möglich. Über einen weiten Wertebereich einstellbare Integrationszeiten erlauben es, das Gerät für verschiedene Meßszenarien zu verwenden. Die Leistungsdaten des aufgebauten Radiometers wurden durch die Ergebnisse von Systemmessungen und durch beispielhafte Feldtests verifiziert.

By Wolfgang Menzel*, Horst Bilzer*, Arnold Gronau*, Ralf Leberer*, Winfried Mayer*, and Rainer Müller**

Für die Dokumentation
Radiometry / Radiometer / Folded Reflect Array Antenna / Circular Waveguide-to-microstrip Transition

1. Introduction

A radiometer is a passive microwave sensor to detect the blackbody radiation of *absorptive* objects and thus to detect the object's temperature. For *real* objects, the received radiation is a superposition of the radiation emitted by the target and radiation reflected from the surrounding. It can be used as a passive surveillance sensor for astronomical research [1], agricultural purposes [2], for environmental protection [2, 3], for security applications [4], or for military missions [5]. Compared to radar, however, radiometry is much less known to the public. Therefore, the 38 GHz radiometer as described in this paper was designed and built as a demonstrator in microwave systems education. In an ideal way, it can be used to teach the topics of noise in microwaves, modern low-noise and high gain receivers, sensor antennas, and some signal processing. In addition, it serves as a test vehicle for different kinds of component technologies as well as for packaging and interconnect technologies in the mm-wave range. The radiometer was realized within a diploma thesis (with contributions from all authors), thus it provided to the student a task with many aspects of industrial work including design of the overall system, of RF and IF components as well as mechanical parts, and it required the coordination of the different own and contributed actions to finally build and test the radiometer.

In chapter 2 of this paper, the architecture and system design are described. In the following chapter, all building blocks of the radiometer are introduced, and design and assembly of an assortment of them is described in detail. A summary of performance data of the radiometer and some exemplary radiometric measurements are given in chapter 4.

2. Architecture and System Design

The principal block diagram of the radiometer is shown in **Fig. 1**. Radiation collected by the antenna is fed to the input of a low noise amplifier (LNA1). To connect the MMIC based microstrip amplifier with the antenna feed (realized as circular waveguide), a special transition as described later on is used. The LNA's output signal passes through a coupler structure to the down-converter. A second input of the coupler is connected to the output of a second low noise amplifier LNA2 with a temperature reference load connected to its input. A thermal sensor closely placed to the reference load and the LNAs is permanently recording the ambient temperature T_A, so that the noise power density of the reference load can be determined by the well known formula $S = k \cdot T_A$. Switching on the two LNAs separately, either the noise power received by the antenna or the noise power provided by the temperature reference is down-converted to the IF band. These noise signals then are amplified in the IF stage, and the power is detected and A/D-converted for further processing in a controller or a personal computer (PC). In the controller, the radiation related temperature T_x is calculated from detector outputs of both the antenna and the reference load taking into account the measured ambient temperature T_A.

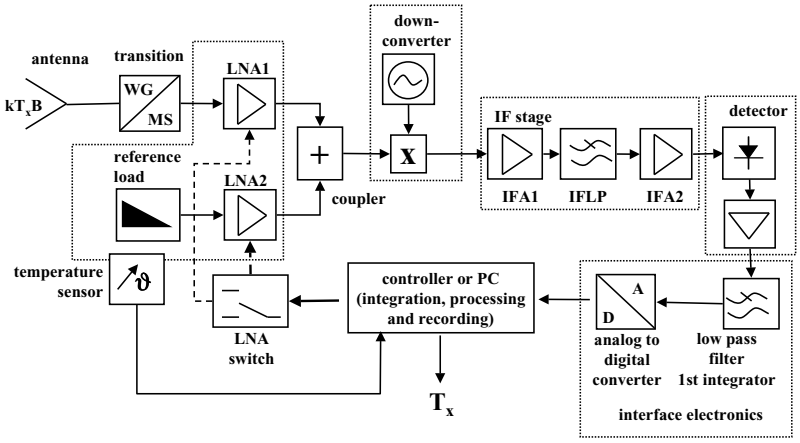

Fig. 1: Simplified block diagram of the radiometer

* University of Ulm, Microwave Techniques, Ulm, Germany
** EADS ewation GmbH, Ulm, Germany

Based on Fig. 1, two equations can be set up to describe the noise power detected from the antenna path N_{ant} (with LNA1 switched on) and from the temperature reference N_{ref} (with LNA2 switched on):

$$N_{ant} = k \cdot T_x \cdot B \cdot G_{sig} + k \cdot \left(F_{sig} - 1\right) \cdot T_A \cdot B \cdot G_{sig} \quad (1)$$

$$N_{ref} = k \cdot T_A \cdot B \cdot G_{ref} + k \cdot \left(F_{ref} - 1\right) \cdot T_A \cdot B \cdot G_{ref}. \quad (2)$$

In this equations, G_{sig}, G_{ref} and F_{sig}, F_{ref} are the gains and noise figures of the two paths, k is the Boltzmann constant, and B the receiver bandwidth (equal for both paths), T_A the ambient temperature of the noise reference and the receiver, and T_x the unknown temperature to be measured.

For a high temperature resolution of the radiometer, a high value for G_{sig} has to be chosen, and it can not be assumed to be constant over temperature. Moreover, due to the receiver noise figure F_{sig}, the contribution of the right term of equation (1) to the noise power N_{ant} is considerably higher than the contribution of the left term containing the measured temperature T_x. So the measurement of T_x from N_{ant} using just equation (1) would clearly be falsified by changes of G_{sig}. This problem is solved using the reference path and equation (2) to eliminate G_{sig}.

Introducing the factors $Y = N_{ant}/N_{ref}$ and $X = G_{ref}/G_{sig}$, equations (1) and (2) can be solved for T_x by

$$T_x = \left(X \cdot Y \cdot F_{ref} - F_{sig} + 1\right) \cdot T_A. \quad (3)$$

Assuming the same noise figures for the two LNAs and a symmetric coupler structure, and taking into account the gain of the waveguide-to-microstrip transition G_{WGMS}, F_{sig} can be expressed by $F_{sig} = F_{ref}/G_{MSWG}$. From the same considerations, X is expressible just by $X = G_{ref}/G_{sig} = 1/G_{MSWG}$. To take into account asymmetries in the LNAs and the coupler structure, X is preferably determined by a calibration measurement with the antenna directed to a microwave absorber at a known ambient temperature. The asymmetries have some influence on the ratio of F_{sig} and F_{ref} as well, but to a negligible extent because of the gain of the LNAs (Friis formula). Changes of the noise figures of the LNAs over temperature are accounted for by a linear temperature coefficient $\delta F(T_A)$ for F_{sig} which has been obtained from temperature tests.

Finally equation (3) is used to determine the noise temperature T_x of the target from two noise power measurements N_{Ant} and N_{ref} and the temperature of the built-in reference load.

For a better understanding of the component descriptions in the subsequent chapters, a power budget of the two paths is provided in the following **table 1**.

Noise temperature resolution of a radiometer is determined by the integration time [6, 7]. Thus it competes with a fast acquisition rate of the radiometer. To be able to use the radiometer for many different test scenarios, adjustable integration times are advantageous. For this radiometer, the first integration element is the low pass filter in front of the analog to digital converter (Fig. 1). Further integration can be done numerically in the controller. Minimum integration time is set by the analogue low pass filter, and integration time is adjustable in integer multiples of the low pass filter time constant of approximately 2 ms.

RF bandwidth of the radiometer is limited by the antenna and the transition to the planar receiver components to approximately 2 GHz. Consequently, the 3 dB cut-off frequency for the IF signal is set to 1 GHz. Because of stability reasons, the IF stage is realized with a bandpass characteristic having a low frequency cut-off of 80 MHz. With a two side band down-converter this results in a small frequency gap in the middle of the RF frequency range, and an overall effective bandwidth of approximately 1.8 GHz is achieved.

3. Components of the Radiometer

3.1 Overview

In **Fig. 2** the complete radiometer assembly is depicted. All millimeter-wave and electronic building blocks are mounted on the back side of the antenna sharing a common base plate. The millimeter-wave assembly, its power supply, and the IF electronics are protected and shielded by an aluminum top cover. To avoid long RF path lengths, all millimeter-wave components are located close to the microstrip-to-waveguide transition which itself is located on top of the antenna feed in the center of the whole assembly. The interface electronics including the analog to digital converter are realized on two separate printed circuit boards mounted beneath the top cover of the millimeter-wave assembly.

In the following sections, details on design and realization of the antenna, the microstrip-to-waveguide transition, the millimeter-wave assembly, and the IF stage are given. In addition, some general information is presented on the interface and on the software.

3.2 Folded Reflector Antenna

Antenna directivity, gain, beamwidth and sidelobe level play an important role with respect to the radiometer system properties like angular resolution, bandwidth, required amplification, signal to noise ratio and temperature resolution.

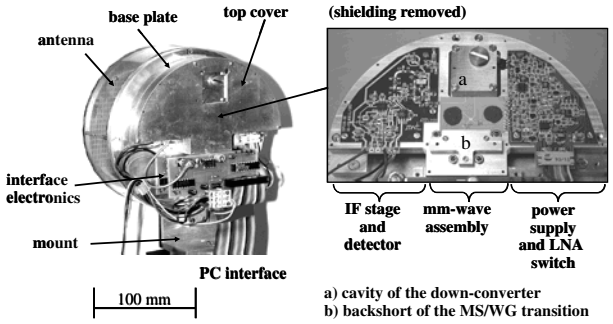

Fig. 2: Photographs of the complete radiometer assembly (left) and the millimeter-wave and IF parts (right) which are covered by an aluminum housing for mechanical protection and shielding

Table 1: Budget plan of the radiometer according to Fig. 1

component	antenna path		reference path		Remarks
	G/dB	F/dB	G/dB	F/dB	
transition MS-WG	–2.6	2.6	–	–	including the microstrip path to the LNA
LNA	20.0	3.5	20.0	3.5	
coupler	–4.0	4.0	–4.0	4.0	
down-converter	–7.0	7.0	–7.0	7.0	taking into account power from two sidebands
if amplifier	40.0	6.0	40.0	6.0	two stages
whole chain	46.4	6.96	49.0	4.36	

In this case, a printed folded reflector antenna [8, 9] with high gain, low profile, low loss and potentially low production cost is used. The basis for the design of the planar reflector is a periodic array of dipoles printed on a dielectric substrate with backside metallization. With a plane wave incident from broadside, the complete power is reflected, the phase angle, however, depends on dipole length and, to a minor degree only, on the dipole width (**Fig. 3**). The reflection behavior of this arrangement is calculated using a spectral domain code. The phase angle calculated from a *periodic* structure even can be used for the design of planar reflector antennas with dipoles on a *periodic grid, but different dimensions.*

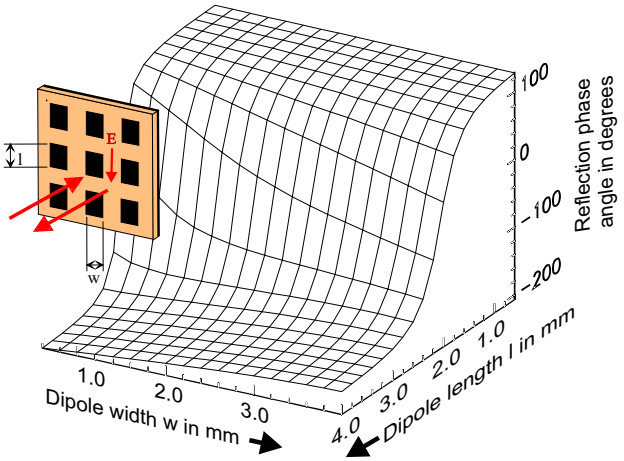

Fig. 3: Periodic array of dipoles and reflection phase angles as a function of dipole geometry

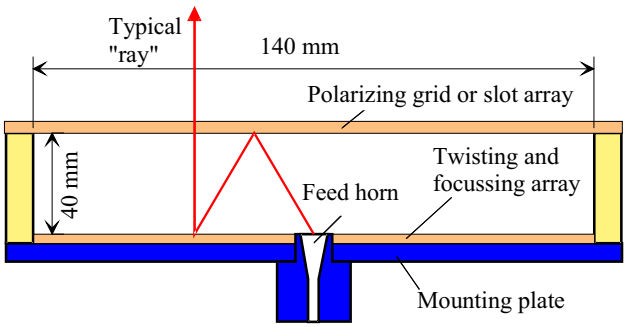

Fig. 4: Basic principle of folded reflector antenna

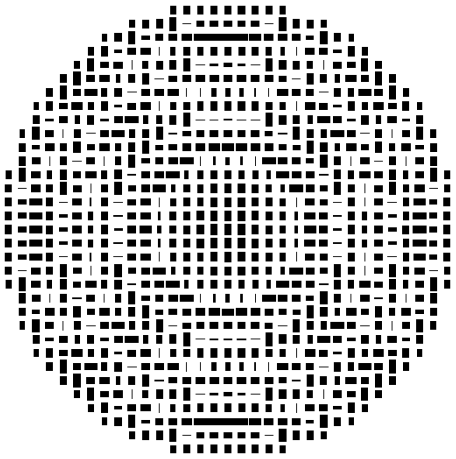

Fig. 5: Layout of a Ka-band reflectarray for folded reflector antennas

Making use of an independent choice of length and width of the printed dipoles, different properties for the two polarizations can be adjusted in this way. The focusing array can be modified to include a polarization twisting of the electromagnetic field, leading, together with a printed polarizing grid, to a folded antenna configuration.

The principle function of a printed and folded reflector antenna is indicated in **Fig. 4**. The radiation of the feed is reflected by a printed polarizer grid at the front of the antenna. Then the wave is incident on the printed reflector, where the dipole axes are tilted by 45° with respect to the incident electric field. The dimensions of the dipoles are designed in such a way that

1. a phase difference of 180° occurs between the two components of the reflected wave parallel to the dipole axes leading to a twisting of the electric field, and
2. an overall phase shift is adjusted according to the focusing requirements.

The outgoing plane wave then can pass the slot array. The design of this antenna once again is done on the basis of a periodic structure. For varying dipole dimensions, the reflection phase angles are calculated for both principal polarizations. The optimum combination of phases then is selected from this set of data according to both twisting and focusing requirements.

The reflectarray (**Fig. 5**) was designed on a 0.508 mm thick RT/Duroid 5880 substrate ($\varepsilon_r = 2.2$), with a diameter of 140 mm, 4.1 mm cell size (overall about 900 dipoles), and a focal distance of 80 mm (40 mm between the two reflectors, respectively). It was designed for the centre frequency of 37.5 GHz. The feeding element is a dual-mode-horn [10] to get symmetric illumination of the reflector (equal beamwidth in the E- and H-plane), low cross-polarization of the feed and a –9 dB taper at the reflector edges (reduction of spillover and sidelobe level).

The radiation diagram at 37.5 GHz for both planes is given in **Fig. 6**, showing beamwidths of 3.9° in the elevation and azimuth plane, and a sidelobe level better than 23 dB below the main beam. The gain was measured to be 32 dBi. Similar performance of the antenna was measured, too, at 36.5 GHz and 38.5 GHz (5.3 % bandwidth). Good performance therefore is achieved even at the at the band edges of the radiometer.

3.3 Transition from Circular Waveguide-to-microstrip Line

A new version of a transition from circular waveguide-to-microstrip line is used to transform the TE_{11}-mode from the antenna feed into a microstrip mode for amplification and processing in the following planar circuit. The setup of the transition is shown in **Fig. 7.** For the 50 Ω microstrip line, a 0.254 mm thin, high frequency substrate with high permittivity (RT/duroid 6010M, $\varepsilon_r = 10.2$) is used. The following receiver circuit is realized on the same substrate, thus no additional transition is needed.

The connecting microstrip is lead through a channel into the circular waveguide and ends in a stub. The channel width and length are designed to stay below cutoff for the TE_{10}-mode. To prevent direct leakage of power from the waveguide, a channel length of about one wavelength is chosen.

To stabilize the thin microstrip stub, it is fixed on a dielectric cylinder (Polymethylmethacrylat (PMMA), $\varepsilon_r = 2.58$, $\tan\delta = 0.0066$) placed in the circular waveguide. This cylinder, at the same time, is used to provide an improved matching of the transition and, if properly fixed, it can serve as a sealing of the waveguide. It supports guiding most of the RF signal directly into the waveguide output (about 3 times more energy is coupled into the direction of the cylinder than into the direction of the backshort). Thus the center frequency for the transition is mainly determined by the length of the cylinder. Increasing this length by multiples of half wavelengths does not change the center frequency but reduces the bandwidth. Along the length of the cylinder,

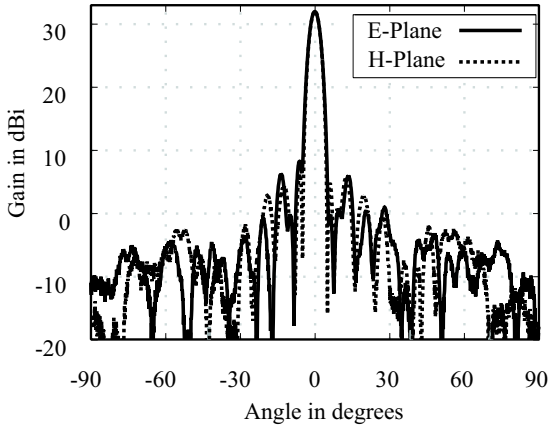

Fig. 6: Radiation diagrams of the Ka-band folded reflector antenna at 37.5 GHz

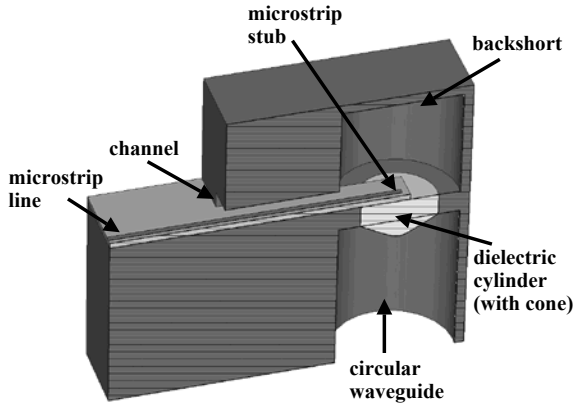

Fig 7: Cut through the transition from microstrip to circular waveguide

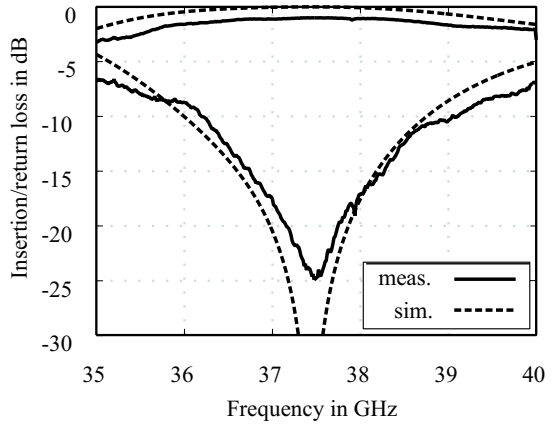

Fig 8: Simulated and measured insertion and return losses of the transition from circular waveguide-to-microstrip

the waveguide diameter is reduced to stay below cutoff for the TM_{01}-mode, but it is kept large enough to minimize dispersion effects. Reshaping the lower flat end of the cylinder to a cone, the bandwidth is increased further. The backshort length has minor effect on the center frequency but on the overall performance of the transition. Best insertion loss was found for a backshort length of about a quarter wavelength. Further improvements of the bandwidth can be realized by

- using material with lower permittivity (and lower losses) for the cylinder,
- increasing the length of the cone, and
- using a small patch instead of a thin stub.

The scattering parameters of the transition were determined measuring two sets of two back-to-back transitions connected by microstrip lines of different length. From this, the scattering parameters of a single transition can been calculated. Simulated [11] and measured results of the transition agree very well (**Fig. 8**). Additional attenuation in the transmission are due to losses in the PMMA cylinder, to substrate losses, and to some spurious radiation at the channel opening. The return loss is lower than –12.5 dB over a bandwidth of 2 GHz.

3.4 Millimeter-Wave Assembly

All active millimeter wave functions of the radiometer are realized using MMICs embedded in a planar hybrid assembly containing lumped and distributed passive elements. Apart from the down-converter, all transmission lines and distributed elements are implemented in microstrip technology on a RT/Duroid 6010M substrate. **Fig. 9** shows the arrangement of the millimeter-wave components.

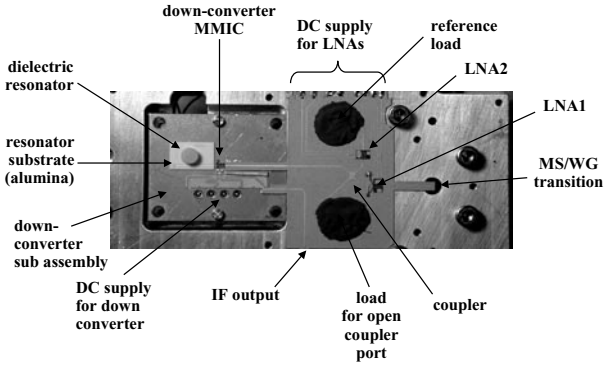

Fig. 9: Photograph of the millimeter-wave assembly. The cavity of the down-converter and the backshort of the MS/WG transition have been removed

The low noise amplifiers LNA1 and LNA2 are commercially available PHEMT GaAs MMICs [12] with a frequency range of 36 GHz to 40 GHz, covering well the operational band of the radiometer. They are fixed by conductive epoxy directly on the base plate in holes of the surrounding substrate. Their RF and DC ports are contacted by bond wires to RF and DC lines on the substrate. For RF blocking single layer capacitors are placed close to each gate- and drain-connection. The LNAs are switched on and off by changing their gate voltages from operational values of –0.3 V to pinch-off values of < –1.3 V.

The down-converter (provided by EADS as a separate sub assembly) is based on a special MMIC [13] including an oscillator for frequencies from 18.5 GHz to 19.5 GHz and a second-harmonic mixer, so that signals in the frequency range from 37 GHz to 39 GHz can be down-converted to IF frequencies from 0.1 GHz to 1.5 GHz. The oscillator is stabilized by a disk shaped dielectric resonator mounted on an alumina substrate according to the data sheet [13]. The whole subassembly is covered by a cubical metal cavity with fixed dimensions necessary to maintain oscillation. The oscillation frequency can be adjusted within some MHz by a screw in the top of the cavity.

3.5 dB Patch Coupler

As fabrication and tolerance requirements prevented the application of a conventional hybrid-ring on the chosen material and for the frequency range used here, a new coupler concept was chosen. The classical hybrid ring was replaced by a rectangular coupling patch [14, 15] modified to meet the required specifications.

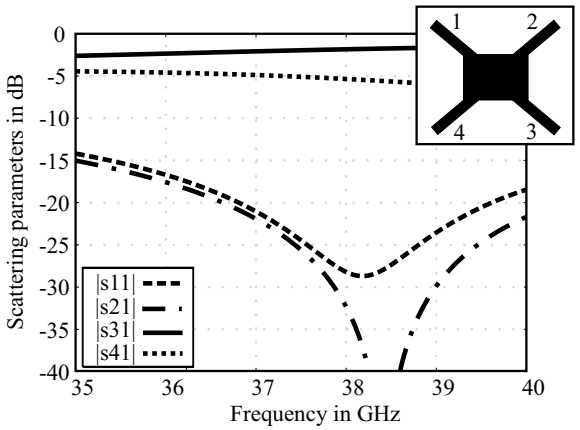

Fig. 10: Simulation results of the unmodified patch coupler

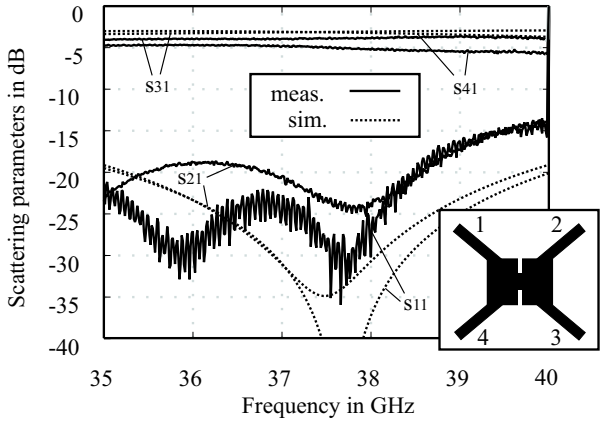

Fig. 11: Comparison of simulation and measurement results of the optimized coupler; (patch length: 1.643 mm, patch width 1.235 mm, slot length: 0.308 mm, slot width: 0.06 mm)

The original patch coupler as shown in **Fig. 10** consists of a rectangular patch with the connecting lines at the edges.

Like all the other millimetre-wave components, the coupler was designed and built up on a RT Duroid 6010M substrate with a substrate height of h = 0.254 mm and a relative permittivity of ε_r = 10.2. ADS Momentum [16] has been used to optimize the 3 dB coupler. The starting values for the optimization were calculated according to the design guidelines in [15]:

$$a = b + w \cdot \sqrt{2} \tag{4}$$

and

$$b = 0.46 \cdot \ddot{e}_{\mathrm{g}} \tag{5}$$

with w microstrip line width, λ_{g} wavelength on the substrate, a patch length, and b patch width.

Simulation results of this coupler (Fig. 10) have shown that with this design, no symmetrical power division can be obtained for the two output ports. As a way out of this problem, slots have been inserted into the long sides of the coupler patch (**Fig. 11**). With this modified design, a symmetric power distribution has been achieved.

Two samples of the coupler have been fabricated and measured with a two-port vector network analyser (VNWA). The remaining two ports were connected to a special matched load as described later on. Commercial coplanar on-waver probes were used to contact the microstrip feed lines of the coupler whereby the ground contacts have been realised with quarter-wave radial stubs [17].

Fig. 11 gives a comparison of the measured and simulated insertion and return losses between the coupled ports. The differences between measurement and simulation result from lossless simulation models. The asymmetric characteristic between the measured insertion loss values $|s_{31}|$ and $|s_{41}|$ is due to fabrication variations in the two coupler assemblies necessary to be able to characterise the structure by two port measurements.

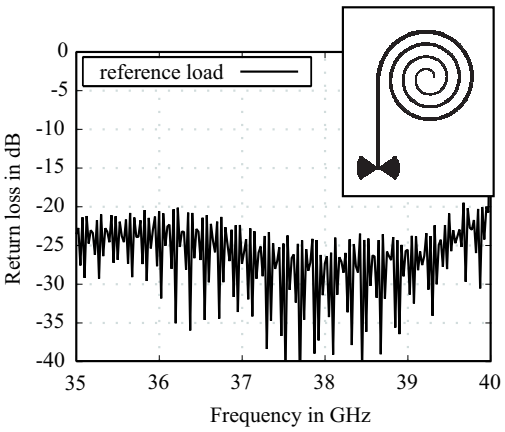

Fig. 12: Measurement results and design of the planar matched load

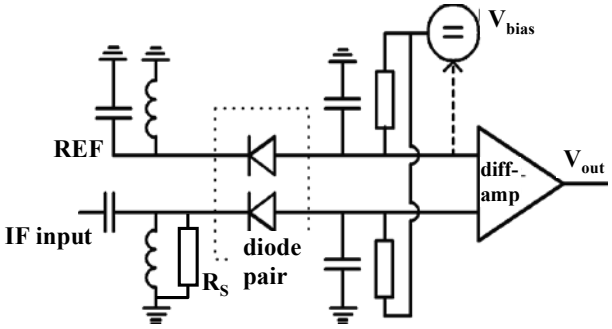

Fig. 13: Simplified circuit of the implemented detector

3.6 Planar Matched Load

For the reference path of the radiometer and for termination of the unused port of the 3 dB patch-coupler, planar matched loads are required. These were realized using microstrip spirals with decreasing line width over length (Fig. 4). Absorbing material [18] is painted on top of the spiral to make it lossy and so to avoid reflections. Number and distance of the turns were experimentally optimized for best return loss. The measurement results show a very low reflection coefficient (**Fig. 12**).

3.7 IF stage and detector

The down-converted noise signal with a power level of approximately –70 dBm and a dynamic range of less than 2 dB has to be amplified and converted to a linear output voltage in the range between 0 V and 4.096 V of an A/D-converter.

Two wideband silicon amplifiers [19] with an overall gain of approximately 40 dB are used to increase the power level (IFA1 and IFA2 in Fig. 1). A 1 GHz low pass filter (IFLP in Fig. 1) with lumped elements is used to limit the noise bandwidth.

For the linear detection (power to voltage conversion) of the amplified and filtered IF signal with its relatively small dynamic range of 2 dB and a wide bandwidth of 10 MHz to 1 GHz, a modified diode detector circuit is used.

Standard Schottky detector diodes without bias normally have a narrow bandwidth characteristic because of their high junction resistance. To improve the input match for the necessary wide bandwidth, a bias of 145 µA is applied to the detector diode, and

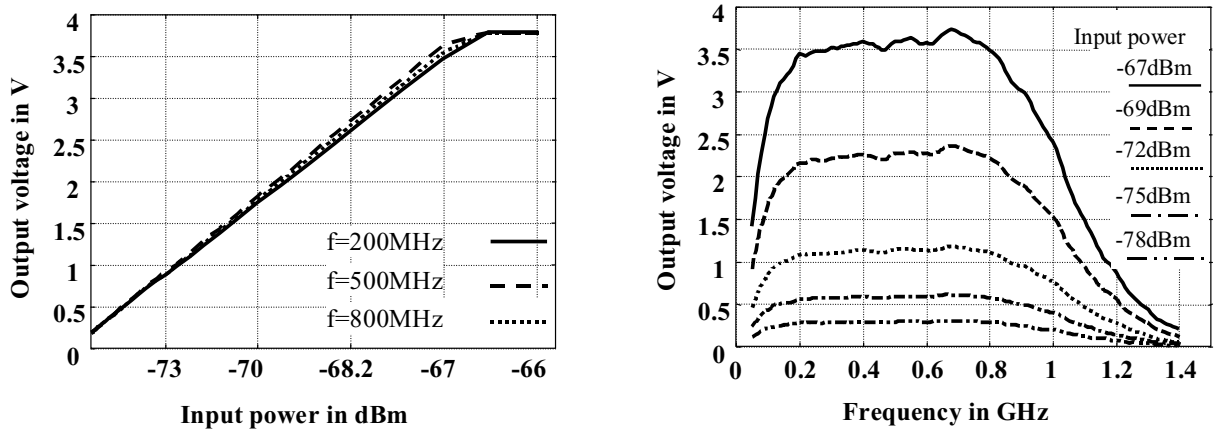

Fig. 14: Measured performance of the IF stage together with the detector showing the power-to-voltage transfer curve (left) and the frequency response for various power levels (right)

Table 2: Measured performance data of the radiometer.

Parameter	Conditions, Explanations	Value
Angular resolution	3 dB beam width in azimuth and elevation	3.9 °
Center frequency		37.53 GHz
Bandwidth		1.8 GHz
noise figure	measured without antenna	7.4 dB
Temperature resolution	for minimum integration time of 2 ms for an integration time of 0.1 s	2.6 K 0.8 K
Measurement range	minimum measurable noise temperature $T_{x,min}$ maximum measurable noise temperature $T_{x,max}$	20 K 500 K
Operating temperature range	changes of T_x < 10 K	15 °C to 40 °C
Sampling rate	for minimum integration time of 2ms (presently limited by the interface)	50 Hz
DC power	currents at + 4.5 V / -4.5 V	< 500 mA / < 50 mA
Size	diameter / depth	150 mm / 90 mm

a shunt resistor R_S (**Fig. 13**) is added to get an input resistance close to 50 Ω.

To compensate the temperature drift of the diode (dependency of the junction resistance on the ambient temperature), a stabilised voltage source V_{bias} (Fig. 13) is implemented to keep the bias voltage constant.

Furthermore, to compensate the output offset voltage before amplifying the detected signal, a reference path with another diode and the same bias was added to the detector circuit, and the signal is further amplified by a differential amplifier. Using a diode pair from the same die, a good match in DC characteristics and temperature drift of the two diodes can be expected.

Fig. 14 shows measurement results of the IF stage and the detector according to the block diagram in Fig. 1. The excellent linearity of the power to voltage conversion for different frequencies can be seen in the left diagram, the amplitude responses for various input power levels are plotted in the right diagram.

3.8 Interface Electronics and Software

With the interface electronics (Fig. 1) and the software it is possible to use the parallel port of a standard PC to operate the radiometer. The interface electronics provides the readout of the output signals of the antenna path, the reference path and the ambient temperature sensor as well as the switching of the low noise amplifiers. It includes two 14 bit precision analog to digital converters with serial output and some digital latches. Due to serial execution of all the measurements and a slow data transmission to the PC, the interface electronics is presently limiting the radiometer sampling rate to 50 Hz.

Data processing and integration of the temperature measurements as well as the recording and storing of measurement data over time is done by a PC based software implemented in C programming language.

4. Performance Data and Test Results

Table 2 summarizes the data obtained from measurements of the complete radiometer assembly. The present overall performance is suitable for different demonstrations and measurements as it is shown by the following two examples. A number of parameters, however, still have to be optimized to better meet the original specifications.

4.1 Application example 1: Traffic monitoring

In a first test, the radiometer has been mounted on a bridge looking to a street below where approximately one lane is illuminated by the antenna lobe (**Fig. 15**). The signal from vehicles passing the antenna lobe is different from the radiation of the asphalt making it possible to detect vehicles by the change of the noise temperature over time. As metal parts of the vehicles are not radiating, they reflect the cold temperatures of the sky ahead of them, resulting in negative deflections in the recorded curves.

4.2 Application example 2: Imaging of a human hand

Using a 2D scanning mechanism and an additional focusing lens to increase local resolution of the antenna, a human hand held in front of a metal sheet has been recorded. **Fig. 16** shows the results of this measurement with intensity coded noise temperatures. Despite of the low differences between the ambient temperature

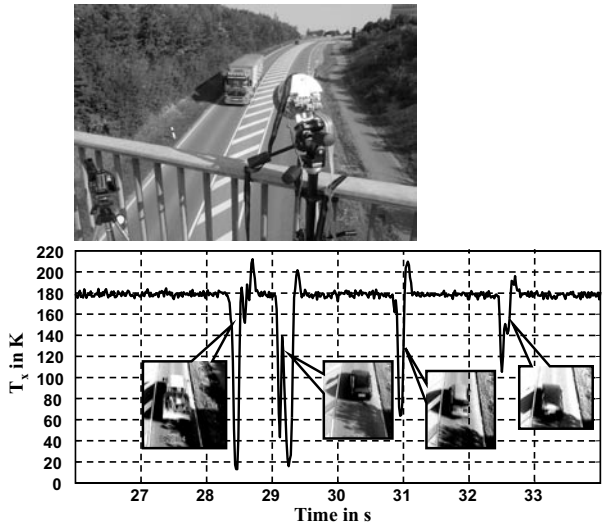

Fig. 15: Photograph of the test arrangement (top) of the first application example and measured noise temperatures of passing vehicles (bottom).
The photographs corresponding to the measured signal deflections were taken from a video camera operated in parallel to the measurement procedure

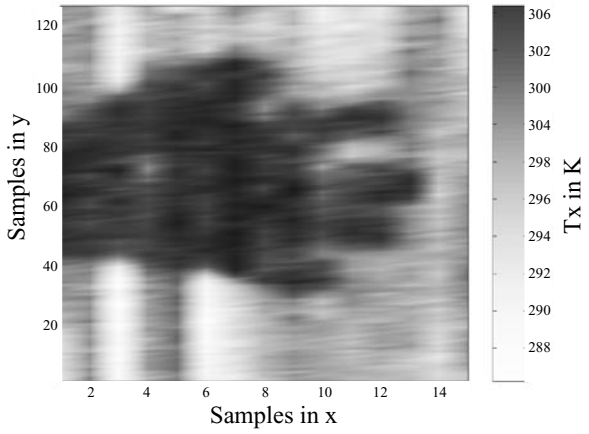

Fig. 16: Planar scan of a human hand held in front of a metal sheet

of the surroundings reflected by the metal sheet and the surface temperature of the skin, the contours of the hand are clearly visible.

5. Conclusion

In this paper, design and first results of a room temperature radiometer at 38 GHz have been demonstrated. The radiometer will serve as demonstration equipment for students and interested people. In addition, it was used to apply and test some novel principles concerning antenna, millimeter-wave components, and interconnect and packaging technology. As a result, a rather compact system (diameter 150 mm, depth 90 mm) was achieved. An internal reference load, receiver temperature sensing and compensation will allow, within a reasonable range of ambient temperatures, the detection of absolute radiation temperatures. To increase sampling rate and to improve temperature resolution, work has been started to replace the interface electronics and parts of the PC based software by an embedded microcontroller.

This works has been supported by component samples and test equipment from EADS Deutschland, Microwave Factory and United Monolithic Semiconductors (UMS).

References

[1] Roddis, N. et al.: Differential radiometer at 30 GHz for the Planck Mission. 3rd ESA Workshop on Millimetre Wave Technology and Applications, Espoo, Finland, May 21–23, 2003, pp. 81–86.
[2] Lüdi, A.: Passive abbildende Systeme im mm-Wellen Bereich. Institut für Angewandte Physik, Universität Bern, IAP-Forschungsbericht Nr. 2000-5 (http://www.iapmw.unibe.ch/publications/pdffiles/188.pdf).
[3] Süss, H.; Grüner, K.; Wilson, W. J.: Passive Millimeter Wave Imaging: A Tool for Remote Sensing. Alta Frequenza, Vol. LVIII, No. 5–6 (1989) pp. 457–465.
[4] Barnes, A. R. et al.: MMIC Technology and its Application in Passive mm-Wave Imaging Systems. 3rd ESA Workshop on Millimetre Wave Technology and Applications, Espoo, Finland, May 21–23, 2003, pp. 543–547.
[5] Appleby, R.; Gleed, D.;Lettington, A.: The Military Applications of Passive Millimetre Wave Imaging. J. Defense Science, Vol. 2, No. 2 (April 1997).
[6] Schiek, B.; Siweris, H.-J.: Rauschen in Hochfrequenzschaltungen. Hüthig Buch Verlag Heidelberg, 1990.
[7] Vowinkel, B.: Passive Mikrowellenradiometrie. Wiesbaden: Vieweg und Sohn Verlagsgesellschaft, 1988.
[8] Pilz, D.; Menzel, W.: Printed mm-wave folded reflector antenna with high gain, low loss, and low profile. Antennas and Propagation Symposium Digest, Vol. 38 (July 2000) pp. 790–793.
[9] Menzel, W.; Pilz, D.; Leberer, R.: A 77 GHz FM/CW radar front-end with a low-profile, low-loss printed antenna. IEEE Trans. on Microw. Theory Tech., Vol MTT-47 No. 12 (Dec. 1999).
[10] Pickett, H. M.; Hardy, J. C.; Farhoomand, J.: Characterization of a Dual-Mode Horn for Submillimeter Wavelengths. IEEE Trans. on MTT, Vol. MTT-32 (1984, pp. 936–937.
[11] CST-Computer Simulation Technology: HF Design and Analysis CST Microwave Studio, 2003.
[12] United Monolithic Semiconductors: 36-40 GHz Low Noise High Gain Amplifier CHA2094b. Data Sheet, 1999.
[13] United Monolithic Semiconductors, K-band Oscillator with integrated Q-band Harmonic Mixer CHV2241. Data Sheet, 2001.
[14] Fusco, V. F.;Merugu, L. N.: Full Wave Analysis of 94 GHz Patch Coupler. IEEE MTT-S Digest, Vol. 2 (1990) pp. 649–652.
[15] Fusco, V. F.; Stewart, J. A. C.: Design and synthesis of patch microwave couplers. European Microwave Conference Proceedings, 1986, pp. 86.401–406.
[16] AGILENT TECHNOLOGIES: ADVANCED DESIGN SYSTEM 2002 C, 2002.
[17] Strauss, G.; Ehret, P.; Menzel, W.: On-wafer measurement of microstrip-based mimics without via holes. IEEE Transactions on Microwave Theory and Techniques Symposium, 1996, pp. 1399-1402.
[18] CUMING MICROWAVE CORPORATION: C-RAM 369, Brushable or Sprayable Surface Wave Suppressor.
[19] Agilent Technologies: Agilent ABA-51563 3.5GHz Broadband Silicon RFIC Amplifier, datasheet February 20, 2003.

Dipl.-Ing. (BA) Winfried Mayer
e-mail: winfried.mayer@ieee.org

Dipl.-Ing. H. Bilzer
e-mail: bilzer@mwt.e-technik.uni-ulm.de

Dipl.-Ing. Ralf Leberer
e-mail:ralf@mwt.e-technik.uni-ulm.de

Dipl.-Ing. (FH) A. Gronau
e-mail: arnold@mwt.e-technik.uni-ulm.de

Prof. Dr.-Ing. W. Menzel
e-mail: menzel@mwt.e-technik.uni-ulm.de

University of Ulm
Microwave Techniques
Albert-Einstein-Allee 41
89069 Ulm
Germany

Dipl.-Ing. Rainer Müller
EADS
ewation GmbH
Woerthstrasse 85
89077 Ulm
Germany
e-mail: rainer.a.mueller@sysde.eads.net

(Received on October 10, 2003)